

Experimental Extraction and Simulation of Charge Trapping during Endurance of FeFET with TiN/HfZrO/SiO₂/Si (MFIS) Gate Structure

Shujing Zhao, Fengbin Tian, Hao Xu, Jinjuan Xiang, Tingting Li, Junshuai Chai, Jiahui Duan, Kai Han, Xiaolei Wang, Wenwu Wang, and Tianchun Ye

Abstract—We investigate the charge trapping during endurance fatigue of FeFET with TiN/Hf_{0.5}Zr_{0.5}O₂/SiO₂/Si (MFIS) gate structure. We propose a method of experimentally extracting the number of trapped charges during the memory operation, by measuring the charges in the metal gate and Si substrate. We verify that the amount of trapped charges increases during the endurance fatigue process. This is the first time that the trapped charges are directly experimentally extracted and verified to increase during endurance fatigue. Moreover, we model the interplay between the trapped charges and ferroelectric polarization switching during endurance fatigue. Through the consistency of experimental results and simulated data, we demonstrate that as the memory window decreases: 1) The ferroelectric characteristic of Hf_{0.5}Zr_{0.5}O₂ is not degraded. 2) The trap density in the upper bandgap of the gate stacks increases. 3) The reason for memory window decrease is increased trapped electrons after program operation but not related to hole trapping/de-trapping. Our work is helpful to study the charge trapping behavior of FeFET and the related endurance fatigue process.

Index Terms—FeFET, Si, ferroelectric, doped HfO₂, endurance fatigue, charge trapping.

I. INTRODUCTION

THE discovery of ferroelectric property in doped HfO₂ rejuvenates the FeFET research activity due to its complete compatibility with Si CMOS technology, scaling potential, and excellent retention property [1-4]. After ~10 years of intensive research, this CMOS-compatible material innovation enabled the demonstration of a FeFET technology scaled to the 28 nm and 22 nm nodes utilizing a conventional high- κ /metal gate

technology [2, 5, 6]. Fast switching speed (≤ 100 ns), switching voltages in the range of 2.5~6 V, and 10-year data retention have been demonstrated for ferroelectric HfO₂ [7]. However, the endurance characteristic of Si FeFET has been limited to be $10^4\sim 10^5$ cycles during the period of 2011~Feb. 2021 [8-19]. Very recently, significantly improved endurance of $>10^{10}$ cycles is reported by using high- κ Si₃N₄ interlayer in replacement of SiO₂ [20]. Meanwhile, the Hf_{0.5}Zr_{0.5}O₂ based Si FinFET with SiO_x interlayer also shows high endurance of $>10^{10}$ cycles [21]. Generally, the endurance of $>10^{14}$ cycles is preferred for the industry's mass production [7]. Thus the Si FeFET endurance is still a key urgent challenge.

The physical origin of endurance fatigue is considered as charge trapping and trap generation [9, 10, 22]. Especially the charge trapping and de-trapping behaviors play dramatic roles [23]. During the program/erase (PGM/ERS) process of doped HfO₂ based Si FeFET, the remnant polarization is generally $10\sim 30$ $\mu\text{C}/\text{cm}^2$. This results in that the electric field across the interfacial layer (SiO₂) ($30\sim 90$ MV/cm) exceeds its breakdown field (<15 MV/cm), which causes significant charge trapping/de-trapping. Thus, the techniques of quantitatively extracting/characterizing the charge trapping amount are rather essential to understand the charge trapping behavior, as well as its role on endurance fatigue.

Generally, there are two kinds of methods to quantitatively evaluate the trapped charges. One kind is directly measuring the trapped charges [24, 25]. This method evaluates the trapped charges by subtracting the substrate charge change from the total charges influent into the substrate. The trapped charges are found to be $\sim 10^{14}$ cm^{-2} [24, 25]. The other kind is by tracing the threshold voltage (V_{th}) shift during the stress and release processes [17, 26-28], similar to the bias temperature instability (BTI) measurement. This method evaluates the trapped charges by considering that the trapped charges induce the V_{th} shift. The trap concentration is about 10^{20} cm^{-3} , and the trap energy band is localized at ~ 1.8 to 2 eV below the conduction band minimum (CBM) of Hf_{0.5}Zr_{0.5}O₂. In addition, there are several other methods to probe the traps, such as low-frequency noise [15, 29], atomic force microscope (AFM) [30], Kelvin probe force microscope (KPFM) [30], trap spectroscopy by charge injection and sensing (TSCIS) [27], and exhaustive photo depopulation spectrum (EPDS) [27]. Even though the above methods have been proposed to investigate the charge trapping

Manuscript received June 30, 2021. This work was supported by the National Natural Science Foundation of China under Grant No. 61904199 and 61904193, and in part by the Open Research Project Fund of State Key Laboratory of ASIC and System under Grant No. KVVH1233021. (Corresponding authors: Hao Xu, Jinjuan Xiang, Junshuai Chai)

Shujing Zhao, Fengbin Tian, Hao Xu, Jinjuan Xiang, Tingting Li, Junshuai Chai, Jiahui Duan, Kai Han, Xiaolei Wang, Wenwu Wang, and Tianchun Ye are with Key Laboratory of Microelectronics Devices and Integrated Technology, Institute of microelectronics, Chinese academy of sciences, Beijing 100029, China. The authors are also with University of Chinese Academy of Sciences, Beijing 100049, China (xuhao@ime.ac.cn; xiangjinjuan@ime.ac.cn; chajunshuai@ime.ac.cn).

Kai Han is with Weifang University, Shandong 261061, China.

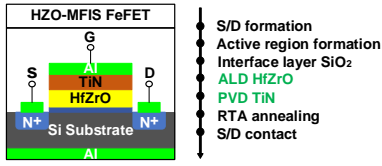


Fig. 1. Schematic of Si FeFET structure and its fabrication process.

behavior, the detailed mechanism of charging trapping induced endurance fatigue is still unclear. Generally, the endurance failure is ascribed to increased trapped charges with increasing PGM/ERS cycles [9, 10, 22, 25, 28]. On the contract, Ichihara *et al.* from Kioxia Corporation directly measured the trapped charges and found that trapped charges decreased with increasing PGM/ERS cycles [24]. Therefore, it is controversial whether the endurance failure is due to the increase of charge trapping. And the detailed physical picture of endurance fatigue by charge trapping is still unclear and consequently needs clarification.

In this work, we investigate the charge trapping during endurance fatigue of FeFET with TiN/Hf_{0.5}Zr_{0.5}O₂/SiO₂/Si (MFIS) gate structure. We propose a method of experimentally quasi-directly extracting the number of trapped charges during the memory operation. The amount of trapped charges increases during the endurance fatigue process. This is the first time that the trapped charges are directly experimentally extracted and verified to increase during endurance fatigue. Moreover, we model the interplay between the trapped charges and ferroelectric polarization switching during the endurance fatigue and give a detailed physical picture of charge trapping induced endurance fatigue.

II. EXPERIMENTAL AND MODEL

A. FeFET fabrication and electrical measurements

Fig. 1 shows a schematic diagram of the Si FeFET structure and its fabrication process. The FeFET was fabricated by the gate-last process. Firstly, the source and drain regions were formed by the As ion implantation for nMOSFET using the energy of 40 keV with a dose of $4 \times 10^{15} \text{ cm}^{-2}$, followed by annealing at 1050 °C for 5 s in N₂ atmosphere. Then the gate stack was grown. After diluted-HF clean, a 0.7 nm SiO₂ interfacial layer was grown by ozone oxidation at 300 °C in the atomic layer deposition (ALD) chamber. Then 9 nm Hf_{0.5}Zr_{0.5}O₂ was grown by ALD at 300 °C. The Hf precursor, Zr precursor, and O source were tetrakis-(ethylmethylamino)-hafnium (TEMA-Hf), tetrakis-(ethylmethylamino)-zirconium (TEMA-Zr), and H₂O, respectively. The 10 nm TiN and 75 nm W were grown by sputtering. Then ferroelectric phase crystallization was achieved by 550 °C for 60 s in N₂ to form orthorhombic phase. After the gate formation, the source/drain contacts were defined by lithography, and TiN/Al was used as contact metal. Finally, forming gas annealing at 450 °C in 5%-H₂/95%-N₂ was performed. In addition, the capacitor of TiN/9 nm Hf_{0.5}Zr_{0.5}O₂/TiN was also fabricated with the same growth condition as the FeFET.

The transfer characteristics I_d - V_g and gate capacitance (C_g) were measured by Keysight B1500A. The polarization hysteresis loop was measured by the Radiant Precision LC ferroelectric tester. For the MFM capacitor, a triangle wave

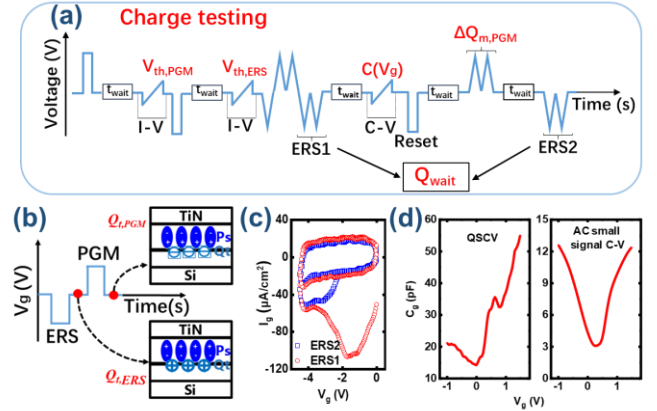


Fig. 2. (a) The method of measuring trapped charges. (b) The typical PGM/ERS operation of FeFET. (c) The measured gate current during the ERS1 and ERS2 processes. (d) Comparison between QSCV and high-frequency small AC signal C-V.

with $\pm 3 \text{ V}$ voltage amplitude at 1 kHz was used for hysteresis loop measurement. A square wave of $\pm 3 \text{ V}$ voltage amplitude at 1 ms width was used for the endurance measurement. For the FeFET, AC small-signal at 100 kHz was used to measure C_g - V_g . A square wave of $\pm 4.5 \text{ V}$ voltage amplitude at 200 μs width was used for the endurance measurement. The threshold voltage was extracted by the linear extrapolation method.

B. Method of measuring trapped charges

Fig. 2(a)-(b) show the method of measuring trapped charges and the typical PGM/ERS operation of FeFET. Generally, electrons are trapped into the gate stack after PGM pulse, and here the trapped charge amount is denoted as $Q_{t,PGM}$. Holes are trapped after ERS pulse, and the trapped charge amount is denoted as $Q_{t,ERS}$. In this work, we experimentally measure the difference between the $Q_{t,PGM}$ and $Q_{t,ERS}$, i.e., $\Delta Q_t = Q_{t,PGM} - Q_{t,ERS}$, which represents the charge trapping behavior.

Next, we give the details of measuring ΔQ_t . For the FeFET device, there are three kinds of free charges, including charges in the metal gate (Q_m), Si substrate (Q_{Si}) and trapped charges (Q_t). Similar to the definition of ΔQ_t , we can define the ΔQ_m and ΔQ_{Si} correspondingly. According to the charge neutrality condition, we can obtain

$$\Delta Q_t + \Delta Q_m + \Delta Q_{Si} = 0 \quad (1)$$

Thus the ΔQ_t can be obtained after knowing the ΔQ_m and ΔQ_{Si} .

The ΔQ_m is experimentally measured as shown in Fig. 2(a). After the negative pulse, two consecutive positive triangular waves are applied. Then the charge change on the metal gate is obtained by integrating the gate current, denoted as $\Delta Q_{m,PGM}$. It should be noted that the second triangular wave is used to eliminate the gate leakage, which is similar to the positive-up-negative-down (PUND) method. During our experimental measurement, we found that an unstable Q_m component appears after the positive pulse, that is, part of Q_m is released. Thus it is necessary to evaluate the amount of unstable Q_m (denoted as Q_{wait}) to exactly obtain the Q_t . The *direct* measurement of Q_{wait} needs a current measurement with a sampling time of fewer than 1 μs , together with a whole measurement time of more than 10 s simultaneously. Thus the *direct* measurement of Q_{wait} is rather difficult. Here we measure the Q_{wait} using the following alternative method as shown in Fig.

2(a). Firstly, after the positive triangular waves, two consecutive negative triangular waves (denoted as ERS1) are applied without waiting time. The charge change on the metal gate during this process ($\Delta Q_{m,ERS1}$) can be obtained by integrating the external current during the ERS1 process. Secondly, after the positive triangular wave and 100 s waiting time, two consecutive negative triangular waves (denoted as ERS2) are applied. The charge change on the metal gate during this process ($\Delta Q_{m,ERS2}$) can be obtained by integrating the external current during the ERS2 process. Here the waiting time of 100 s is used to ensure that the unstable charges are fully released. Fig. 2(c) shows the measured current during the above two processes. It can be seen that a current peak disappears for the ERS2 process compared with the ERS1 process. This indicates that the Q_{wait} are released during the 100 s waiting time. Finally, the Q_{wait} are determined as

$$Q_{wait} = \Delta Q_{m,ERS2} - \Delta Q_{m,ERS1} \quad (2)$$

Then the stable component (ΔQ_m) can be obtained as

$$\Delta Q_m = \Delta Q_{m,PGM} - Q_{wait} \quad (3)$$

Then the ΔQ_{Si} is experimentally measured. After the PGM pulse, the substrate charge magnitude $Q_{Si,PGM}$ can be obtained if the V_{th} and C_g-V_g are known as

$$Q_{Si,PGM} = \int_0^{V_{th,PGM}} C_{g,PGM}(V_g) dV_g \quad (4)$$

where $C_{g,PGM}$ means the gate capacitance after PGM pulse. Similarly, after the ERS pulse, the substrate charge magnitude $Q_{Si,ERS}$ can be obtained as

$$Q_{Si,ERS} = \int_0^{V_{th,ERS}} C_{g,ERS}(V_g) dV_g \quad (5)$$

Then the ΔQ_{Si} can be obtained as

$$\begin{aligned} \Delta Q_{Si} &= Q_{Si,PGM} - Q_{Si,ERS} \\ &= \int_0^{V_{th,PGM}} C_{g,PGM}(V_g) dV_g - \int_0^{V_{th,ERS}} C_{g,ERS}(V_g) dV_g \\ &= \int_{\Delta V_{th}}^{V_{th,ERS}} C_{g,ERS}(V_g) dV_g - \int_0^{V_{th,ERS}} C_{g,ERS}(V_g) dV_g \\ &= -\int_0^{\Delta V_{th}} C_{g,ERS}(V_g) dV_g \end{aligned} \quad (6)$$

Finally, the ΔQ_t can be obtained from (1).

In addition, the spontaneous polarization change (denoted as ΔP_S) corresponding to ΔQ_t process can be evaluated. The V_{th} shift due to ΔQ_t and ΔP_S can be given as

$$\Delta V_{th} = -\frac{\Delta Q_t + \Delta P_S}{C_{FE}} = -\frac{\Delta Q_t + \Delta P_S}{\epsilon_0 \epsilon_{FE}} d_{FE} \quad (7)$$

where C_{FE} means the ferroelectric capacitance. The ϵ_0 and ϵ_{FE} represent vacuum and relative dielectric constants of ferroelectric, respectively. d_{FE} means the physical thickness of ferroelectric. Then the ΔP_S can be known as

$$\Delta P_S = \Delta Q_t - \frac{\epsilon_0 \epsilon_{FE}}{d_{FE}} \Delta V_{th} \quad (8)$$

It should be noted that our method is based on the work by Ichihara *et al.* from Kioxia Corporation [24]. Their method can use one-time current measurement to extract the ΔQ_t . However, there are two issues about their method. Firstly, their method overestimates the ΔQ_{Si} . They measured the C_g-V_g by the direct current method, in other words, quasi-static C_g-V_g (QSCV). Thus the measured C_g contains the contribution from ferroelectric spontaneous polarization switching. The C_g and resulted ΔQ_{Si} are overestimated. While in our work, we use the high-frequency small AC signal to measure the C_g-V_g . This can

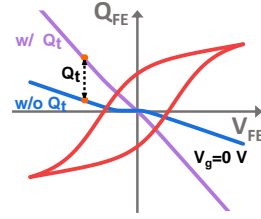


Fig. 3. The effect of charge trapping on loadline.

significantly suppress the ferroelectric contribution. Moreover, we also experimentally compared the two methods. We found that the ΔQ_{Si} obtained by the QSCV method is 71.1% larger than that by the AC method, the C_g-V_g curve shown in Fig. 2(d). Similar results have been reported [17], which further supports the above discussion. Secondly, their method results in overestimated ΔQ_m . Their method measured the Q_{wait} with an additional triangle wave for I_d-V_g test. This induced additional electron trapping and consequently underestimated Q_{wait} . We found that the ΔQ_m obtained with an additional triangle wave is 5.6% larger than that without an additional triangle wave (not shown here). While in our method, we independently measure Q_{wait} and $V_{th,PGM}$ to remove the additional triangle wave, and can more accurately evaluate the ΔQ_m .

C. Modeling of MFIS gate stack with charge trapping

We model voltage and charge distribution across the MFIS gate stack by using the polarization-electric field curve ($P-E_{FE}$) of ferroelectric and loadline curve, based on our previous work [31]. The hysteresis loop of the ferroelectric is described by the Miller model. The loadline is given as

$$\begin{aligned} V_{FE} &= V_g - \psi_S - V_{IL} = V_g - \psi_S + \frac{Q_{Si}(\psi_S)}{\epsilon_0 \epsilon_{IL}} t_{IL} \\ &= V_g - \psi_S - \frac{Q_m(\psi_S) + Q_t(\psi_S)}{\epsilon_0 \epsilon_{IL}} t_{IL} \end{aligned} \quad (9)$$

where the ϵ_0 and ϵ_{IL} represent vacuum and relative dielectric constants of the interlayer, respectively. t_{IL} means the physical thickness of the interlayer. The term $Q(\psi_S)$ means that the Q is a function of ψ_S . The (9) has used the (1). From the (9), we can obtain a V_{FE} value for each ψ_S at a given V_g . Then the $Q_m(\psi_S)$ vs. V_{FE} curve, i.e., the loadline, can be obtained.

We discuss the relationship between the Q_t and ψ_S . The charge trapping/de-trapping occurs during the PGM/ERS process. The occupation of traps is influenced by the relative position between the trap energy levels and Fermi level. Thus, as ψ_S and V_{IL} increases, the negative trapped charges Q_t becomes larger. Similarly, as ψ_S and V_{IL} decreases, the positive trapped charges Q_t becomes larger.

We discuss the role of $Q_t(\psi_S)$ on the loadline. The introduction of Q_t will cause the loadline to become steeper. The reason is given as follows. Here we explain the case of negative charge trapping. At a given V_g , for the same V_{FE} condition, the ψ_S is identical no matter of with and without negative trapped charges. With identical ψ_S , Q_m increases due to the negative trapped charges base on (1). Thus the point on the loadline shifts upwards when negative charges are trapped, as shown in Fig. 3. With decreasing the V_{FE} , more negative charges are trapped, resulting in a larger upward shift. Therefore the loadline becomes steeper. For the case of positive charge trapping the conclusion is same.

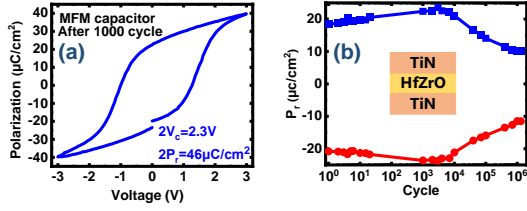


Fig. 4. (a) P-V of the $\text{Hf}_{0.5}\text{Zr}_{0.5}\text{O}_2$ MFM capacitor after 10^3 PGM/ERS cycles and (b) the endurance process.

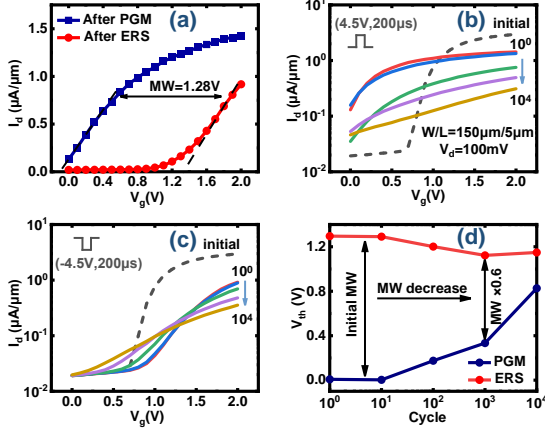


Fig. 5. (a) I_d - V_g curve after (a) wake up, and after (b) PGM and (c) ERS during the endurance process. (d) The MW. This device is woken up after 1s, $\pm 4.5\text{V}$ pulse.

Based on the model we can calculate voltage and charge distribution across the MFIS gate stack, especially the ΔQ_t and ΔQ_m , and compare them with the experimental results.

III. RESULTS AND DISCUSSION

A. Polarization characteristics of $\text{Hf}_{0.5}\text{Zr}_{0.5}\text{O}_2$ ferroelectric

Fig. 4(a) shows the P-V curve of the $\text{Hf}_{0.5}\text{Zr}_{0.5}\text{O}_2$ MFM capacitor after 10^3 PGM/ERS cycles. The remnant polarization $2P_r$ is about $46 \mu\text{C}/\text{cm}^2$, and coercive voltage $2V_c$ is about 2.3 V (coercive field $2E_c \sim 2.6 \text{ MV}/\text{cm}$). Fig. 4(b) shows the endurance process. When the cycle number increases from 10^0 to 10^4 , the $2P_r$ increases from 36 to $46 \mu\text{C}/\text{cm}^2$. From 10^4 to 10^6 , $2P_r$ decreases. Thus the ferroelectric characteristic of the MFM capacitor does not degrade until 10^4 cycles.

B. Endurance fatigue of $\text{Hf}_{0.5}\text{Zr}_{0.5}\text{O}_2$ FeFET

Fig. 5(a) shows the I_d - V_g curve after wake up. The memory window (MW) is 1.28 V . Fig. 5(b) and (c) show I_d - V_g curves during the endurance process. The V_{th} can be extracted and the MW is shown in Fig. 5(d). The MW decreases with increasing the PGM/ERS cycle. After 10^3 cycles, the MW is reduced to be 60%. After 10^4 cycles, the MW is reduced to be 20%. After 10^5 cycles, the MW disappeared. From the endurance difference between the MFM capacitor and FeFET, we can conclude that the charge trapping plays a dramatic role on the FeFET, which is consistent with the reported results [9, 10, 16, 22, 25, 26].

C. Quantitative characterization of charge trapping during the endurance fatigue process

Firstly, we experimentally investigate the ΔQ_m . Fig. 6(a)

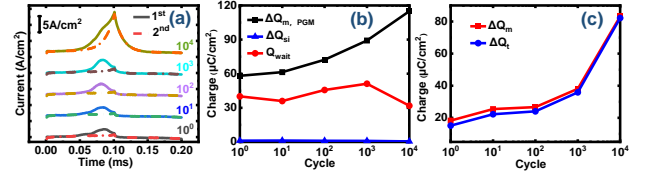


Fig. 6. (a) External current during two consecutive positive triangular waves. (b) $\Delta Q_{m,PGM}$, Q_{wait} and ΔQ_{Si} during endurance fatigue. (c) ΔQ_m and ΔQ_t during endurance fatigue.

shows external current during two consecutive positive triangular waves (see Fig. 2(a)). The current corresponding to the 1st triangular wave is larger than the 2nd one. This indicates the ferroelectric spontaneous polarization reversal. Then the $\Delta Q_{m,PGM}$ is obtained as shown in Fig. 6(b). The $\Delta Q_{m,PGM}$ increases from 58 to $114 \mu\text{C}/\text{cm}^2$ as the PGM/ERS cycle increases. The Q_{wait} is also shown in Fig. 6(b). The Q_{wait} does not change significantly and is about $40 \mu\text{C}/\text{cm}^2$. It indicates that the trap density corresponding to unstable charge trapping is not changed significantly. Finally, the ΔQ_m is obtained as shown in Fig. 6(c). The ΔQ_m increases from 18 to $83 \mu\text{C}/\text{cm}^2$ as the PGM/ERS cycle increases. The leakage current across the gate stack increases during the endurance fatigue process as shown in Fig. 6(a). The maximum leakage increases from $5 \mu\text{A}$ after 10^0 cycle to $87 \mu\text{A}$ after 10^4 cycles. This indicates that significant defect generation process occurs.

Secondly, we experimentally investigate the ΔQ_{Si} . The ΔQ_{Si} can be obtained based on (6), and shown in Fig. 6(b). The ΔQ_{Si} decreases from 3.15 to $0.93 \mu\text{C}/\text{cm}^2$ due to MW reduction.

Finally, we experimentally investigate the ΔQ_t , as shown in Fig. 6(c). The ΔQ_t significantly increases, from $17 \mu\text{C}/\text{cm}^2$ after 10^0 cycle to $80 \mu\text{C}/\text{cm}^2$ after 10^4 cycles. Considering that the surface potential difference between the two states after PGM and ERS pulse decreases during the endurance fatigue, the increase in ΔQ_t is caused by the increase of density of the stable trap of the gate stack. Furthermore, we conclude that the endurance fatigue is originated from the increase of ΔQ_t .

It should be noted that our work directly verifies that the trapped charges increase during endurance fatigue for the first time. For the method of evaluating the trapped charges by tracing the V_{th} [17, 26-28], it cannot directly measure the trapped charges. Considering that the endurance fatigue could also originate from the fatigue of ferroelectric, this method can only speculatively ascribe endurance fatigue to the charge trapping behavior. For the method of directly measuring the trapped charges, it found that the trapped charges decreased during endurance fatigue [24]. Thus charge trapping cannot be considered as the origin based on their results. Our method evaluates the charge trapping behavior experimentally and directly. We find that the trapped charges increase during endurance fatigue. Thus it is the first time to credibly report the enhancement of charge trapping during endurance fatigue.

D. Simulation results

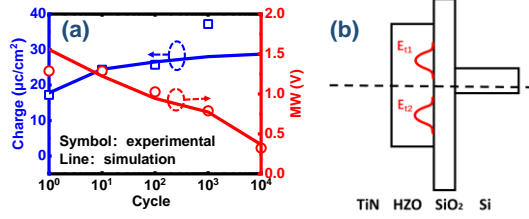


Fig. 7. (a) Experimental and simulation results of the MW and ΔQ_i . (b) Schematic of the traps at FE/DE interface.

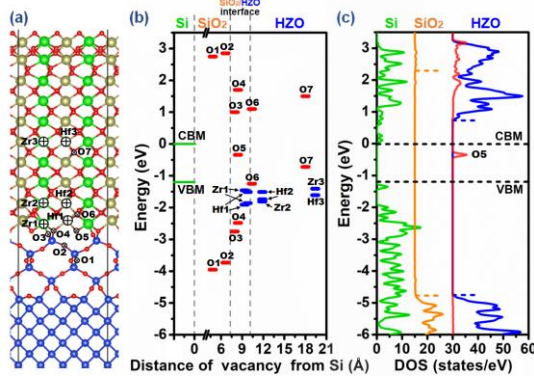


Fig. 8. (a) The Hf_{0.5}Zr_{0.5}O₂/SiO₂/Si gate stack model. The “⊕” and “⊗” represent metal and O atom vacancies, respectively. Several physical positions of metal or O vacancy are considered. (b) The energy level distribution of vacancy defects. (c) The projected density of states for the case of O5 vacancy defect.

To further understand how the charge trapping degrades the endurance characteristic, we simulate the relationship between the trapped charge and the endurance fatigue process. Fig. 7(a) shows the experimental results about the MW and trapped charges ΔQ_i , together with the simulated data. It can be seen that the experimental and simulated data are well consistent. This indicates the validity of the modeling. The parameters in our modeling are determined as follows. The ferroelectric characteristic parameters (remnant polarization (23 $\mu\text{C}/\text{cm}^2$), saturated spontaneous polarization (30.2 $\mu\text{C}/\text{cm}^2$), and coercive field (1.28 MV/cm)) were determined by fitting the P - V characteristics of the MFM structure. In addition, the ferroelectric characteristic parameters were considered unchanged during the endurance fatigue of FeFET. This is supported by Fig. 4(b), where no ferroelectric degradation appears until 10⁴ cycles. Then these parameters were introduced into the modeling to obtain information about the trap distribution and generation. Based on our consistent modeling of experimental results as shown in Fig. 7(a), we find that the traps at Hf_{0.5}Zr_{0.5}O₂/SiO₂ interface are localized with two energy levels, as shown in Fig. 7(b). One energy position is 0.36 eV above the CBM of the Si substrate (denoted as E_{t1}), and the other is 0.76 eV below the valence band minimum (VBM) of the Si substrate (denoted as E_{t2}). The trap position based on our work is consistent with published results [17, 27]. Moreover, the density of E_{t1} increases from 1×10¹⁴ cm⁻² after 1 PGM/ERS cycle to 3.6×10¹⁴ cm⁻² after 10⁴ cycles. Whereas the density of E_{t2} is nearly unchanged during the endurance fatigue (~1×10¹⁴ cm⁻²). This is consistent with Fig. 5(b), where the V_{th} after ERS operation is nearly unchanged and the V_{th} after PGM operation increases with increasing endurance cycles. Furthermore, to determine the physical origin of traps, we

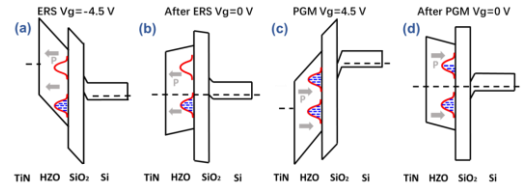


Fig. 9. Energy band diagram (a) at ERS, (b) after ERS, (c) at PGM, and (d) after PGM.

construct a Hf_{0.5}Zr_{0.5}O₂/SiO₂/Si gate stack structure (see Fig. 8(a)) and investigate the distribution of trap energy levels by calculating the projected density of state (DOS) (see Fig. 8(b) and 8(c)) based on *ab initio* calculations employing the HSE06 method [32-34]. It can be seen that the trap energy level near the CBM is mainly contributed to the two-coordinated O atom vacancy at the Hf_{0.5}Zr_{0.5}O₂/SiO₂ interface, while the trap energy level at about 0.65 eV below the VBM is mainly from the metal atom vacancies near the Hf_{0.5}Zr_{0.5}O₂/SiO₂ interface (Hf1, Hf2, Zr1, Zr2) and in the Hf_{0.5}Zr_{0.5}O₂ bulk (Hf3). Thus the E_{t1} is considered to originate from two-coordinated O atom vacancy at the Hf_{0.5}Zr_{0.5}O₂/SiO₂ interface, and the E_{t2} is considered to originate from metal vacancies at the Hf_{0.5}Zr_{0.5}O₂/SiO₂ interface and in Hf_{0.5}Zr_{0.5}O₂ bulk.

Then we discuss the detailed physical picture of charge trapping induced endurance fatigue, based on our modeling. Fig. 9(a) shows the energy band diagram *at* ERS condition. The Fermi level is localized above the E_{t2} trap bands and below the E_{t1} trap bands. Thus the E_{t2} trap bands are occupied by electrons and the E_{t1} trap bands are empty. In addition, the Hf_{0.5}Zr_{0.5}O₂ is negatively polarized. Fig. 9(b) shows the energy band diagram *after* ERS condition. The Fermi level is localized between the E_{t1} and E_{t2} trap bands. Thus the charge trapping is nearly identical between Fig. 9(a) and 9(b). In addition, the Hf_{0.5}Zr_{0.5}O₂ is negatively polarized. Moreover, our modeling finds that the energy band diagram for the ERS operation is similar during the fatigue process. Therefore, the V_{th} is nearly unchanged for the ERS operation. For the PGM operation, Fig. 9(c) shows the energy band diagram *at* PGM condition. The Fermi level is localized above the E_{t1} trap bands. Thus both the E_{t1} and E_{t2} trap bands are occupied by electrons. In addition, the Hf_{0.5}Zr_{0.5}O₂ is positively polarized. Fig. 9(d) shows the energy band diagram *after* PGM. The Fermi level is localized between the E_{t1} and E_{t2} trap bands. However, the trapped electrons in the E_{t1} trap bands cannot fully be de-trapped. In addition, the Hf_{0.5}Zr_{0.5}O₂ is positively polarized. Moreover, our modeling finds that the E_{t1} traps increases during endurance fatigue. Therefore, the V_{th} increases during endurance fatigue. In conclusion, the endurance fatigue of Hf_{0.5}Zr_{0.5}O₂ Si FeFET is due to the increased charge trapping in the upper trap bands.

IV. CONCLUSION

This work presents a method to quantitatively characterize charge trapping of FeFET with TiN/HfZrO/SiO₂/Si gate structure, and studies the detailed physical mechanism of how the charge trapping causes fatigue degradation. We experimentally verify that the amount of trapped charges increases during the endurance fatigue process. This is the first time that the trapped charges are directly experimentally extracted and verified to increase during endurance fatigue.

Moreover, we model the charge trapping and its role in endurance fatigue. We find that the endurance fatigue of FeFET is not due to the fatigue of $\text{Hf}_{0.5}\text{Zr}_{0.5}\text{O}_2$ ferroelectric property, but the increased trap density in the upper energy bandgap. Our work gives a detailed physical picture of endurance fatigue by charge trapping. Our work clearly verifies the charge trapping as the physical origin of endurance fatigue.

REFERENCES

- [1] T. S. Böske et al., "Ferroelectricity in hafnium oxide: CMOS compatible ferroelectric field effect transistors," in *2011 International Electron Devices Meeting*, 2011, pp. 24.5.1-24.5.4. doi:10.1109/IEDM.2011.6131606.
- [2] E. T. Breyer et al., "Reconfigurable NAND/NOR logic gates in 28 nm HKMG and 22 nm FD-SOI FeFET technology," in *2017 IEEE International Electron Devices Meeting (IEDM)*, 2017, pp. 28.5.1-28.5.4. doi:10.1109/IEDM.2017.8268471.
- [3] J. Müller et al., "Ferroelectricity in HfO₂ enables nonvolatile data storage in 28 nm HKMG," in *2012 Symposium on VLSI Technology (VLSIT)*, 2012, pp. 25-26. doi:10.1109/VLSIT.2012.6242443.
- [4] J. Müller et al., "Ferroelectric hafnium oxide: A CMOS-compatible and highly scalable approach to future ferroelectric memories," in *2013 IEEE International Electron Devices Meeting*, 2013, pp. 10.8.1-10.8.4. doi:10.1109/IEDM.2013.6724605.
- [5] S. Dünkel et al., "A FeFET based super-low-power ultra-fast embedded NVM technology for 22nm FDSOI and beyond," in *2017 IEEE International Electron Devices Meeting (IEDM)*, 2017, pp. 19.7.1-19.7.4. doi:10.1109/IEDM.2017.8268425.
- [6] M. Trentzsch et al., "A 28nm HKMG super low power embedded NVM technology based on ferroelectric FETs," in *2016 IEEE International Electron Devices Meeting (IEDM)*, 2016, pp. 11.5.1-11.5.4. doi:10.1109/IEDM.2016.7838397.
- [7] Agarwal et al., "International Roadmap of Devices and Systems 2020 Edition: Beyond CMOS".
- [8] H. Mulaosmanovic et al., "Evidence of single domain switching in hafnium oxide based FeFETs: Enabler for multi-level FeFET memory cells," in *2015 IEEE International Electron Devices Meeting (IEDM)*, 2015, pp. 26.8.1-26.8.3. doi:10.1109/IEDM.2015.7409777.
- [9] E. Yurchuk et al., "Charge-Trapping Phenomena in HfO₂-Based FeFET-Type Nonvolatile Memories," *IEEE Transactions on Electron Devices*, vol. 63, no. 9, pp. 3501-3507, 2016. doi: 10.1109/TED.2016.2588439.
- [10] N. Gong and T.-P. Ma, "A Study of Endurance Issues in HfO₂-Based Ferroelectric Field Effect Transistors: Charge Trapping and Trap Generation," *IEEE Electron Device Letters*, vol. 39, no. 1, pp. 15-18, 2018. doi: 10.1109/led.2017.2776263.
- [11] T. Ali et al., "High Endurance Ferroelectric Hafnium Oxide-Based FeFET Memory Without Retention Penalty," *IEEE Transactions on Electron Devices*, vol. 65, no. 9, pp. 3769-3774, 2018. doi: 10.1109/ted.2018.2856818.
- [12] S. Oh et al., "Improved Endurance of HfO₂-Based Metal-Ferroelectric-Insulator-Silicon Structure by High-Pressure Hydrogen Annealing," *IEEE Electron Device Letters*, vol. 40, no. 7, pp. 1092-1095, 2019. doi: 10.1109/led.2019.2914700.
- [13] H. Mulaosmanovic et al., "Recovery of Cycling Endurance Failure in Ferroelectric FETs by Self-Heating," *IEEE Electron Device Letters*, vol. 40, no. 2, pp. 216-219, 2019. doi: 10.1109/LED.2018.2889412.
- [14] T. Ali et al., "A Multilevel FeFET Memory Device based on Laminated HSO and HZO Ferroelectric Layers for High-Density Storage," in *2019 IEEE International Electron Devices Meeting (IEDM)*, 2019, pp. 28.7.1-28.7.4. doi:10.1109/IEDM19573.2019.8993642.
- [15] H. Bae et al., "Sub-ns Polarization Switching in 25nm FE FinFET toward Post CPU and Spatial-Energetic Mapping of Traps for Enhanced Endurance," in *2020 IEEE International Electron Devices Meeting (IEDM)*, 2020, pp. 31.3.1-31.3.4. doi:10.1109/IEDM13553.2020.9372076.
- [16] C. Y. Chan et al., "FeFET Memory Featuring Large Memory Window and Robust Endurance of Long-Pulse Cycling by Interface Engineering using High-k AlON," in *2020 IEEE Symposium on VLSI Technology*, 2020, pp. 1-2. doi:10.1109/VLSITechnology18217.2020.9265103.
- [17] S. Deng et al., "Examination of the Interplay Between Polarization Switching and Charge Trapping in Ferroelectric FET," in *2020 IEEE International Electron Devices Meeting (IEDM)*, 2020, pp. 4.4.1-4.4.4. doi:10.1109/IEDM13553.2020.9371999.
- [18] S. Deng et al., "Guidelines for Ferroelectric FET Reliability Optimization: Charge Matching," *IEEE Electron Device Letters*, vol. 41, no. 9, pp. 1348-1351, 2020. doi: 10.1109/LED.2020.3011037.
- [19] A. J. Tan et al., "Hot Electrons as the Dominant Source of Degradation for Sub-5nm HZO FeFETs," in *2020 IEEE Symposium on VLSI Technology*, 2020, pp. 1-2. doi:10.1109/VLSITechnology18217.2020.9265067.
- [20] A. J. Tan et al., "Ferroelectric HfO₂ Memory Transistors with High-k Interfacial Layer and Write Endurance Exceeding 1010 Cycles," *IEEE Electron Device Letters*, pp. 1-1, 2021. doi: 10.1109/LED.2021.3083219.
- [21] Sourav De, D. D. Lu, Hoang-Hiep Le et al., "Ultra-Low Power Robust 3bit/cell Hf_{0.5}Zr_{0.5}O₂ Ferroelectric FinFET with High Endurance for Advanced Computing-In-Memory Technology," 2021.
- [22] E. Yurchuk et al., "Origin of the endurance degradation in the novel HfO₂-based 1T ferroelectric non-volatile memories," in *2014 IEEE International Reliability Physics Symposium*, 2014, pp. 2E.5.1-2E.5.5. doi:10.1109/IRPS.2014.6860603.
- [23] J. Li et al., "Quantitative Characterization of Ferroelectric/Dielectric Interface Traps by Pulse Measurements," *IEEE Transactions on Electron Devices*, vol. 68, no. 3, pp. 1214-1220, 2021. doi: 10.1109/TED.2021.3053497.
- [24] R. Ichihara et al., "Re-Examination of V_{th} Window and Reliability in HfO₂ FeFET Based on the Direct Extraction of Spontaneous Polarization and Trap Charge during Memory Operation," in *2020 IEEE Symposium on VLSI Technology*, 2020, pp. 1-2. doi:10.1109/VLSITechnology18217.2020.9265055.
- [25] K. Toprasertpong et al., "Direct Observation of Interface Charge Behaviors in FeFET by Quasi-Static Split C-V and Hall Techniques: Revealing FeFET Operation," in *2019 IEEE International Electron Devices Meeting (IEDM)*, 2019, pp. 23.7.1-23.7.4. doi:10.1109/IEDM19573.2019.8993664.
- [26] Y. Higashi et al., "Impact of Charge trapping on Imprint and its Recovery in HfO₂ based FeFET," in *2019 IEEE International Electron Devices Meeting (IEDM)*, 2019, pp. 15.6.1-15.6.4. doi:10.1109/IEDM19573.2019.8993472.
- [27] B. J. O'Sullivan et al., "Defect profiling in FeFET Si:HfO₂ layers," *Applied Physics Letters*, vol. 117, no. 20, p. 203504, 2020/11/16. 2020. doi: 10.1063/5.0029072.
- [28] M. N. K. Alam et al., "On the Characterization and Separation of Trapping and Ferroelectric Behavior in HfZrO FET," *IEEE Journal of the Electron Devices Society*, vol. 7, pp. 855-862, 2019. doi: 10.1109/JEDS.2019.2902953.
- [29] E. Simoen et al., "Low-frequency noise assessment of ferro-electric field-effect transistors with Si-doped HfO₂ gate dielectric," *AIP Advances*, vol. 11, no. 1, p. 015219, 2021/01/01. 2021. doi: 10.1063/5.0029833.
- [30] U. Celano et al., "Probing the Evolution of Electrically Active Defects in Doped Ferroelectric HfO₂ during Wake-Up and Fatigue," in *2020 IEEE Symposium on VLSI Technology*, 2020, pp. 1-2. doi:10.1109/VLSITechnology18217.2020.9265098.
- [31] X. Wang et al., "Impact of Charges at Ferroelectric/Interlayer Interface on Depolarization Field of Ferroelectric FET With Metal/Ferroelectric/Interlayer/Si Gate-Stack," *IEEE Transactions on Electron Devices*, vol. 67, no. 10, pp. 4500-4506, 2020. doi: 10.1109/TED.2020.3017569.
- [32] G. Kresse and J. J. P. R. B. Hafner, "Ab initio molecular dynamics for liquid metals," *Phys. Rev. B*, vol. 47, no. 1, p. 558, 1993. doi: 10.1103/PhysRevB.47.558.
- [33] G. Kresse and J. J. P. r. B. Furthmüller, "Efficient iterative schemes for ab initio total-energy calculations using a plane-wave basis set," *Phys. Rev. B*, vol. 54, no. 16, p. 11169, 1996. doi: 10.1103/PhysRevB.54.11169.
- [34] J. Heyd et al., "Hybrid functionals based on a screened Coulomb potential," *The Journal of Chemical Physics*, vol. 118, no. 18, pp. 8207-8215, 2003/05/08. 2003. doi: 10.1063/1.1564060.